Preparation and Characterization of Monodisperse Magnetic Carbon Microspheres with Controllable Shell Thickness and High Water Solubility

IOP Conf. Series: Materials Science and Engineering **562** (2019) 012022 doi:10.1088/1757-899X/562/1/012022

Preparation and Characterization of Monodisperse Magnetic Carbon Microspheres with Controllable Shell Thickness and High Water Solubility

Shengji Liang, Kui Chen*, Jinling Han and Bin Wu

School of Chemical Engineering, East China University of Science and Technology, 130 Meilong Road, Shanghai, China
Email:alex_lsj@foxmail.com, chenkui@ecust.edu.cn

Abstract. Core-shell magnetic carbon microspheres with good monodispersity and uniformity were obtained. Good monodispersity was achieved by adding a dispersant in the solvothermal synthesis of magnetic core, as the criterion for good dispersibility was set up through dynamic light scattering (DLS). The excellent dispersing agent (Poly (4-styrenesulfonic acid-co-maleic acid, SS: MA = 3:1) sodium salt, PSSMA) has been selected among three dispersants, which greatly improves the dispersibility of the magnetic core in the coating environment, thereby obtaining a core-shell structure with uniform coating and monodispersity. Carbon shell was gained by deposit coating process of resorcinol formaldehyde resin (RF) onto the magnetic core and then subsequent carbonization under N_2 atmosphere. At the same time, the carbon shell thickness can be adjusted up to 70 nm by adjusting the RF shell thickness which is tunable ranging from 30 to120 nm.

1. Introduction

Fe_3O_4/carbon composite is highly concerned because its function has been so significantly enhanced that makes it fit for great application potential in the fields of electrode materials,[1] magnetic drug targets,[2-4] magnetic resonance imaging contrast agents[5] and etc. Fe_3O_4/C composite has a variety of structural forms, among which core-shell structure is most common.[6-10]

This core-shell composite[11-12] is generally accomplished by a two-step process in which Fe_3O_4 is firstly obtained and then the surface shell. The magnetic core Fe_3O_4 can be obtained by the solvothermal method, by which magnetic particles always have high magnetic saturation strength and good crystallinity. The coating material can be polymers such as nanostructured phenolic resin via surface deposition method.[13-14] As a kind common polymer as well as carbon precursor, nanostructured phenolic resin can be transformed into carbon material with similar morphology after carbonization. It also has various synthetic methods to choose from and has the advantages of easy-to-control structure and high carbon conversion rate.[15-16] Subsequently, Fe_3O_4@C is obtained by calcination under N_2 atmosphere.

However, after Fe_3O_4 is coated by shell material, the composite material often exhibits an obvious agglomeration which is not conducive to the redistribution of materials in the liquid environment.[17] Hence, it is worth noting that before the coating process, the synthesis of Fe_3O_4 nanoparticles of relatively even particle size as core material and its uniform dispersion in the coating environment are key factors. Because the coating environment in which the phenolic resin is synthesized is an aqueous solution, so Fe_3O_4 particles having good hydrophilicity and good dispersion in water is one of the keys to obtaining a finely-coated Fe_3O_4@C core-shell structure with uniform particle size.

The preparation in this study was based on solvothermal synthesis of Fe_3O_4, subsequent in-situ polymerization of resorcinol (R) and formaldehyde (F) and formation of coating resin on the surface of Fe_3O_4 particles to obtain Fe_3O_4@RF microspheres. Then through carbonization, Fe_3O_4@C composite microspheres were produced. And in order to overcome random agglomerates of Fe_3O_4 in the coating environment, an improvement was made by adding a dispersant during the solvothermal synthesis of Fe_3O_4, which was one of our focuses. In this paper, three dispersants, polyethylene glycol (PEG2000), trisodium citrate (Na_3Cit), and poly (styrenesulfonic acid-co-maleic acid) sodium (PSSMA) were compared and dynamic light scattering (DLS) was used as a means of measuring dispersancy effectiveness.[18-20] And the effect and mechanism of dispersants on the dispersion of Fe_3O_4 secondary particles in the aqueous environment were given. As another focus, the manipulation on shell thickness were studied. The carbon shell thickness can be controllable by adjusting resorcinol-formaldehyde resin (RF) thickness which ranges from 30 to 120nm. At the same time, the products at each stage were characterized using transmission electron microscope (TEM), Fourier transform infrared spectroscopy (FTIR), thermogravimetric analysis (TGA), dynamic light scattering (DLS), vibration magnetometer (VM).

2. Experiment

2.1. Preparation of Samples

The bare Fe_3O_4 particles were prepared through a solvothermal method, as described in a previous report.[20] Based on this method, three different dispersants were added respectively during the preparation process.

Dispersion of Fe_3O_4 in water at a certain concentration was characterized by DLS in order to measure its dispersion effect, thus, determining the most effective dispersant.

0.75 g Fe_3O_4 particles above were transferred into a mixture of deionized water (80 mL) and absolute ethanol (32 mL). Then ammonia aqueous solution (NH_4OH, 0.4 mL, 25 wt %) was added and stirred for about 30 min. Subsequently, a certain amount of resorcinol (R) and then formaldehyde solution (F) were added to the reaction solution and stirred for 24 h at 40°C. The formulations of 0.2g R+0.28 mL F, 0.4g R+0.56 mL F and 0.6g R+0.84 mL F are corresponding to Fe_3O_4@RF-1, Fe_3O_4@RF-2, Fe_3O_4@RF-3, respectively. The solid product was collected by a magnet, washed by deionized water and ethanol for three times, and then air-dried at 60 °C for 10 h. The transformation from Fe_3O_4@RF to Fe_3O_4@C was achieved by carbonization method, in which materials were heated to 600 °C under N_2 atmosphere at a heating rate of 2 °C· min^{-1} and then maintained at 600 °C for 4 h. In this way, Fe_3O_4@C-1, Fe_3O_4@C-2 and Fe_3O_4@C-3 were obtained.

2.2. Characterization

The hydrodynamic size and zeta potential of particles, as well as polydispersity index(PDI) were measured on Anton Paar Litesizer 500 (Austria) with a 658 nm laser. Fourier transform infrared spectroscopy (FTIR) spectra of a sample in KBr pellet were recorded on a PerkinElmer Spectrum 100 (The US). Transmission electron microscope (TEM) images were obtained with a JEOL JEM 2100F instrument with an accelerating voltage of 200 KV. Thermogravimetric analysis (TGA) of the samples was conducted with a PerkinElmer TGA-400 instrument (The US) from 30 to 800 °C under an air atmosphere at a heating rate of 10 °C ·min^{-1}. Magnetization hysteresis curve was measured at room temperature in a magnetic field ranging from -20000 Oe to 20000 Oe, by using vibration magnetometer from Quantum Design PPMS (The US).

3. Results and Discussions

3.1. Choice of Dispersant During Solvothermal Synthesis of Fe_3O_4

Three different dispersants (PEG2000, Na_3Cit and PSSMA) were compared in terms of polydispersity index(PDI) of respective Fe_3O_4 suspension liquid, which reflected dispersibility of Fe_3O_4 in water.

Dynamic light scattering (DLS) is a technique based on measuring the fluctuations in the intensity of light scattered from particles in a solution without perturbing the system.[21] From Table 1, without

dispersant participating in the solvothermal process (No.1), the Polydispersity index (PDI) value is greater than 20%. It means that the obtained Fe_3O_4 is not uniform in size and the water dispersion is not stable and easy to precipitate which are in line with the actual performance. This may be the reason why Z-average is up to 2456 nm. Z-average is cumulative hydrodynamic diameter on which large aggregations have greater influence. All of above are probably because the electrostatic repulsion forces are not large enough for them to be dispersed in water.

According to Table 1, after adding dispersant, the PDI value and Z-average of Fe_3O_4 all decrease to a certain extent. And it is worth noting that No.4 has much smaller Z-average and PDI value than No.2 and No.3 do, which means dispersant PSSMA is more effective than PEG2000 and Na_3Cit.

The participation of dispersant also makes mean zeta potential increase. This may explain the reason why mean zeta potential in No.2, 3, 4 is much more negative than it is in No.1 as shown in Table 1. PEG, as a non-ionic dispersant, comes into play which mainly result from steric hindrance because of its huge molecular weight.

Table 1. Synthesis condition and corresponding hydrodynamic size of Fe_3O_4

No.	Additive	Amount/g	Z-average/nm	PDI/%	Mean zeta potential/mV
1	/	/	2456±38	24.2±2.4	-10.3
2	PEG2000	0.5	1914±25	16.9±1.8	-17.9
3	Na_3Cit	0.2	1172±19	19.9±1.7	-20.9
4	PSSMA	0.1	342±8	7.6±0.9	-19.4

* The other conditions of the above experiments are the same: solvent EG dosage 20 mL, NaAc 1.2 g, $FeCl_3 \cdot 6H_2O$ 0.68 g, reaction temperature 200 °C, reaction time 10 h.

Na_3Cit contains three carboxylic acid groups (-COO-), which has a strong coordination with ferric ions.[18] This interaction causes citrate ions to be adsorbed onto the surface of magnetic nanoparticles and thus preventing interparticle aggregation by electrostatic action. Anionic PSSMA contains both sulfonate ($-SO_3^-$) and carboxylate groups (-COO-) which are used as electrostatic stabilizer. PSSMA, as polyelectrolyte, is also characterized by its steric hindrance. Because PSSMA has both electrostatic action and steric hindrance in effect while PEG2000 or Na_3Cit has only one of the two. That's the reason why PSSMA is more effective than the other two.

Concluded from above, PSSMA was chosen for further research. Then the amount of PSSMA was optimized.

In Table 2, No. a, b, c, d are named as Fe_3O_4/PSSMA-0.1, Fe_3O_4/PSSMA-0.3, Fe_3O_4/PSSMA-0.5, Fe_3O_4/PSSMA-1.0. It can be seen from Table 2, as the amount of PSSMA increases, the dispersion effect is slightly improved (as shown in PDI column), but there is no big difference. The Z-average decreases and the mean zeta potential becomes more negative which indicate more PSSMA molecules are adsorbed and winding around Fe_3O_4, making them more negatively charged, thus preventing particles from agglomerating into large particles through electrostatic repulsion and steric hindrance.

Table 2. The influence of PSSMA's amount on corresponding hydrodynamic size of Fe_3O_4

No.	Additive	Amount/g	Z-average/nm	PDI/%	Mean zeta potential/mV
a	PSSMA	0.1	342±8	7.6±0.9	-19.4
b	PSSMA	0.3	305±5	4.2±1.1	-20.5
c	PSSMA	0.5	215±6	6.0±0.9	-22.7
d	PSSMA	1.0	198±6	7.4±0.8	-23.3

* The other conditions of the above experiments are the same: solvent EG dosage 20 mL, NaAc 1.2 g, $FeCl_3 \cdot 6H_2O$ 0.68 g, reaction temperature 200 °C, reaction time 10 h

Figure 1 shows the thermogravimetric curve of Fe_3O_4 with different amounts of PSSMA added in the synthetic process. It can be seen that the increase in the dosage of PSSMA leads to increased coating on the surface of Fe_3O_4, while the cover thickness does not increase unlimitedly. When PSSMA's amount is more than 0.3g, its specific gravity tends to increase very slowly.

After comprehensively comparing the above results, the amount of 0.3 g of PSSMA was selected as the formulation for the later synthesis of Fe_3O_4.

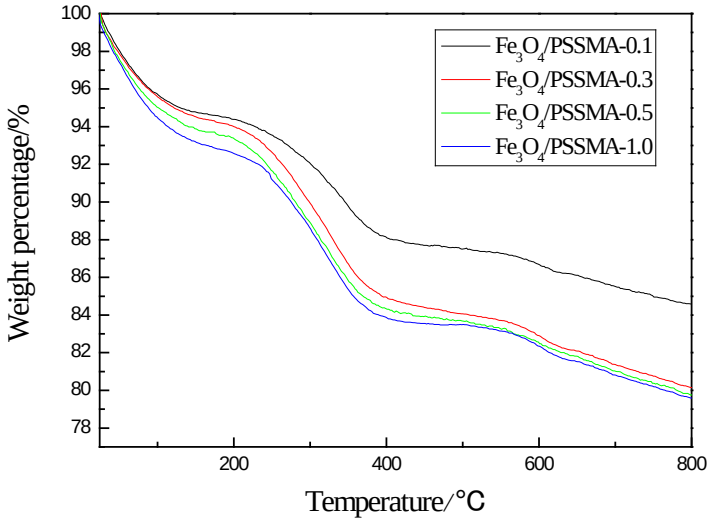

Figure 1. The thermogravimetric curve of Fe_3O_4 with different amounts of PSSMA participating in the synthesis reaction

3.2. Characterization of Fe_3O_4, Fe_3O_4@RF and Fe_3O_4@C

3.2.1. FT-IR spectroscopy

The FT-IR spectra of bare Fe_3O_4, Fe_3O_4/PSSMA (take Fe_3O_4/PSSMA-0.3 as an example), Fe_3O_4@RF, Fe_3O_4@C, RF nanospheres as reference are given in Figure 2.

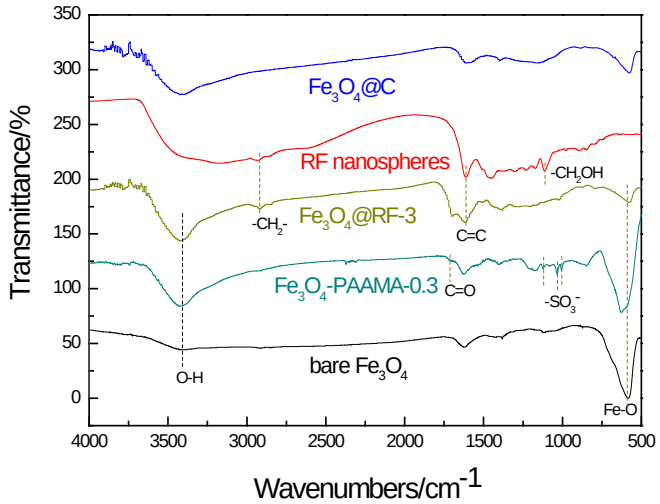

Figure 2. The FT-IR spectra of bare Fe_3O_4, Fe_3O_4/PSSMA-0.3, Fe_3O_4@RF, RF, Fe_3O_4@C nanospheres, respectively

In the spectrum of bare Fe_3O_4, the absorption at 586 cm^{-1} is assigned to the characteristic band of the Fe-O group. The band at 3410 cm^{-1} assigned to the O-H stretching vibration is not very obvious,

which is coincident with the fact that the bare Fe_3O_4 without PSSMA stabilization doesn't show great hydrophilicity.

For Fe_3O_4/PSSMA, the PSSMA-stabilized Fe_3O_4 exhibits characteristic absorption peaks at 1124 cm^{-1}, 1028 cm^{-1} and 1008 cm^{-1} due to sulfonate group from PSSMA, and peak at 1710 cm^{-1} due to stretching vibration of the carbonyl group from PSSMA. In addition, a broad band at 3410 cm^{-1} assigned to the O-H stretching vibration can been clearly seen, which mainly results from carboxylate groups of PSSMA. All of these account for its super hydrophilicity.

For RF nanospheres, the peak at 1612 cm^{-1} is attributed to C=C vibration from benzene ring and peak at 1110 cm^{-1} stretching vibration from hydroxymethyl group. The band around 2923 cm^{-1} is due to the stretching of $-CH_2-$ vibrations. For Fe_3O_4@RF, it can be seen that the similar bands as RF's, which means the composite nanoparticles contain RF. In the same time, the characteristic band of Fe-O group at 570 cm^{-1} is much weaker than that without RF, which is a powerful proof for its core-shell structure.

3.2.2. TEM analysis

Figure 3 presents TEM images of Fe_3O_4@RF, the images show that Fe_3O_4@RF has clear core-shell structure with an average diameter of about 400 nm. The thickness of RF shell can be tunable by adjusting the usage of resorcinol and formaldehyde solution. The images of Fe_3O_4@RF with different shell thickness are shown in Figure 5, Fe_3O_4@RF-1 (a, b), Fe_3O_4@RF-2 (c, d) and Fe_3O_4@RF-3 (e, f) respectively. It can be concluded that an increase in the dosage of resorcinol and formaldehyde solution leads to an increased RF shell thickness. More importantly, the as-prepared products still maintain great monodispersity.

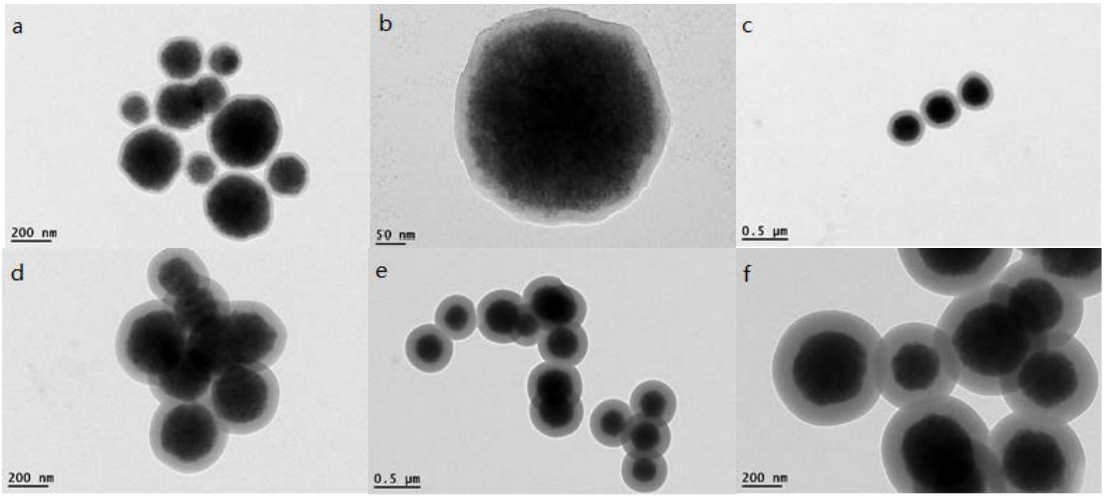

Figure 3. TEM images of Fe_3O_4@RF-1 (a, b), Fe_3O_4@RF-2 (c, d), Fe_3O_4@RF-3 (e, f), respectively

Figure 4 compares the TEM images of Fe_3O_4@RF-3 and Fe_3O_4@C-3. The differences before and after carbonization can be observed. After carbonization, the particle morphology keeps unchanged and no further agglomeration occurs. The thickness of the shell gets slightly thinner, due to the loss during carbonization.

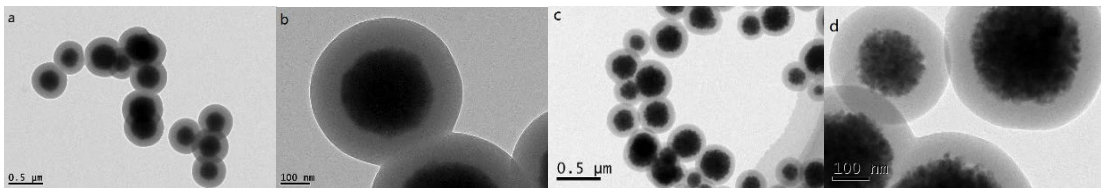

Figure 4. TEM images of Fe_3O_4@RF-3 (a, b), Fe_3O_4@C-3 (c, d), respectively

3.2.3. Thermogravimetric analysis

Figure 5 is the TGA line chart of Fe_3O_4@RF-1, Fe_3O_4@RF-2, Fe_3O_4@RF-3, respectively. The results are consistent with the images of TEM. The more resorcinol and formaldehyde solution added, the thicker RF shell will be. The proportion of Fe_3O_4 core by weight is about 65 % (Fe_3O_4@RF-1), 47 % (Fe_3O_4@RF-2), 39 % (Fe_3O_4@RF-3).

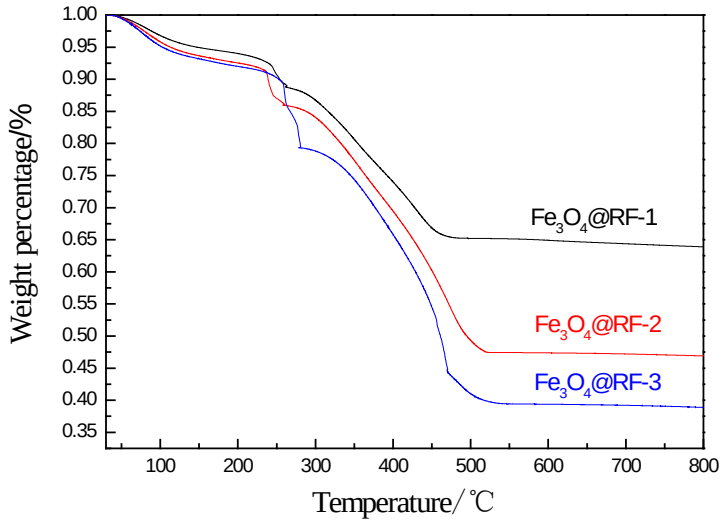

Figure 5. TGA line charts of Fe_3O_4@RF-1, Fe_3O_4@RF-2, Fe_3O_4@RF-3, respectively

3.2.4. Magnetization analysis

As can be seen from Table 3, the saturation magnetization of bare Fe_3O_4 is 74 emu/g, Fe_3O_4/PSSMA-0.3 55 emu/g, Fe_3O_4@RF-3 28 emu/g and Fe_3O_4@C-3 40 emu/g. It can be explained that the PSSMA and then RF shell weaken the magnetism due to their deposition onto the surface of magnetic nanoparticles. After carbonization, the RF shell transforms into carbon shell. The carbon skeleton remains after the escape of hydrogen and oxygen. The weight decreases and the coating thickness gets thinner. That maybe the reason why the saturation magnetization of Fe_3O_4@C-3 is higher than that of Fe_3O_4@RF-3.

Coercivity and residual magnetism of bare Fe_3O_4, Fe_3O_4/PSSMA-0.3, Fe_3O_4@RF-3 and Fe_3O_4@C-3 are shown in Table 3, respectively. After heat treatment, the coercivity has increased dramatically and residual magnetism slightly gets enhanced. This may be attributed to the fact that the magnetic nanoparticles undergo a phase change during heat treatment, and the originally disordered crystal structure is transformed into a crystal structure with high coercivity. Another reason may be the decomposition of dispersant PSSMA during heat treatment, resulting in particle growth and agglomeration. Fe_3O_4 exhibits paramagnetism only in a certain scale range, smaller than 20 nm. This also explains the reason why bare Fe_3O_4, Fe_3O_4/PSSMA-0.3, Fe_3O_4@RF-3 have characteristics close to paramagnetism while Fe_3O_4@C-3 has soft magnetic properties.

Table 3. Magnetic performance data of different samples

No.	Sample	Saturation magnetization/ emu/g	Coercivity/ Oe	Residual magnetism/ emu/g
1	bare Fe_3O_4	74	7	0.9
2	Fe_3O_4/PSSMA-0.3	55	13	1.6
3	Fe_3O_4@RF-3	28	11	0.4
4	Fe_3O_4@C-3	40	174	5.3

4. Summary and Conclusion

In this paper, the dispersing agent was added in the process of solvothermal synthesis of Fe_3O_4 to order to improve the monodispersity of Fe_3O_4 in the later coating environment. By comparison, PSSMA with the best dispersion performance was selected finally and then optimized on its usage. Proper process parameters for the synthesis of Fe_3O_4 have been determined. In the coating process, the thickness of Fe_3O_4@RF shell layer can be conveniently adjusted by controlling the dosage of resorcinol (R) and formaldehyde (F) as monomers, and the thickness of RF shell layer was in the range of 30-120 nm. The composite sphere still maintains its good monodispersity. Fe_3O_4@RF is transformed into Fe_3O_4@C after carbonization process. Super hydrophilicity, monodispersity, good biocompatibility and rapid magnetic separation endow Fe_3O_4@C with application potential in the fields of electrochemistry, adsorption separation and biomedicine.

5. Acknowledgements

we gratefully acknowledge the support provided by Shanghai Committee of Science and Technology, China(Grant No.18595800900) and Anton Paar GmbH.

6. Reference

[1] Li L, Wang T, Zhang L, Su Z, Wang C and Wang R 2012 *Chem. Eur. J.* **18**, 11417-22
[2] Lin C, Ruan W, Zou B, Liu Y and Wang Y 2017 *Acta. Boimater.* **58**, 432-41
[3] Gong X, Peng S, Wen W, Sheng P and Li W 2009 *Adv. Funct. Mater.* **19**, 292-7
[4] Gao Y, Chang M W, Ahmad Z and Li J S 2016 *RSC Adv.* **6**, 88157-67
[5] Zhao G, Wang J, Peng X, Li Y, Yuan X and Ma Y 2014 *Chem. Asian. J.* **9**, 546-53
[6] Wang Z, Guo H, Yu Y and He N 2006 *J. Magn. Magn. Mater.* **302**, 397-404
[7] Guo L, Cui X, Li Y, He Q, Zhang L, Bu W and Shi J 2009 *Chem. Asian. J.* **4**, 1480-5
[8] Li M, Li W and Liu S 2012 *J. Mater. Res.* **27**, 1117-23
[9] Xu S, Tang L, Bi C, Wang X and Lv Y 2010 *Luminescence.* **25**, 294-9
[10] Choi S H, Ko Y N, Jung K Y and Kang Y C 2015 *Chem. Eur. J.* **20**, 11078-83
[11] Caruso F 2010 *Adv. Mater.* **13**, 11-22
[12] Correa-Duarte M A, Grzelczak M, Salgueiriño-Maceira V, Giersig M, Liz-Marzan L M, Farle M, Sierazdki K and Diaz R 2005 *J. Phys. Chem. B.* **109**, 19060-3
[13] Zhang S, Niu H, Hu Z, Cai Y and Shi Y 2010 *J. Chromatogr. A.* **1217**, 4757-64
[14] Li S K, Huang F Z, Wang Y, Shen Y H, Qiu L G, Xie A J and Xu S J 2011 *J. Mater. Chem.* **21**, 7459-66
[15] Liu J, Qiao S, Liu H, Chen J, Orpe A, Zhao D and Lu G 2011 *Angew. Chem. Int. Edit.* **50**, 5947-51
[16] Zhang H, Noonan O, Huang X, Yang Y, Xu C, Zhou L and Yu C 2016 *ACS Nano.* **10**, 4579
[17] Khazaei A, Moosavi-Zare A R, Gholami F and Khakyzadeh V 2016 *Appl. Organomet. Chem.* **30**, 691-4
[18] Liu J, Sun Z, Deng Y, Zou Y, Li C, Guo X, Xiong L, Gao Y, Li F and Zhao D 2009 *Angew. Chem. Int. Edit.* **48**, 5875-9
[19] Deng H, Li X, Peng Q, Wang X, Chen J and Li Y 2005 *Angew. Chem.* **117**, 2842-6
[20] Gao J, Ran X, Shi C, Cheng H, Cheng T and Su Y 2013 *Nanoscale.* **5**, 7026-33
[21] Li S, Xing D and Li J 2004 *J. Biol. Phys.* **30**, 313-24